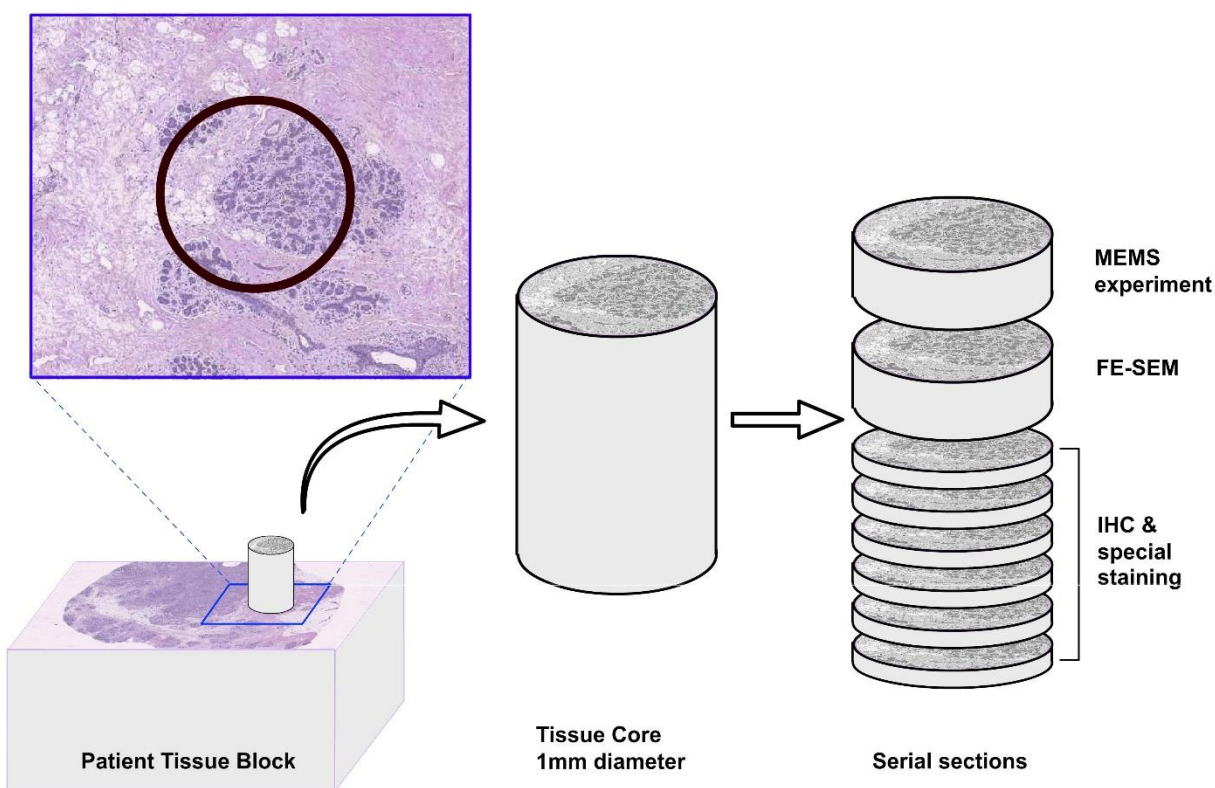


Simultaneous MEMS-based electro-mechanical phenotyping of breast cancer

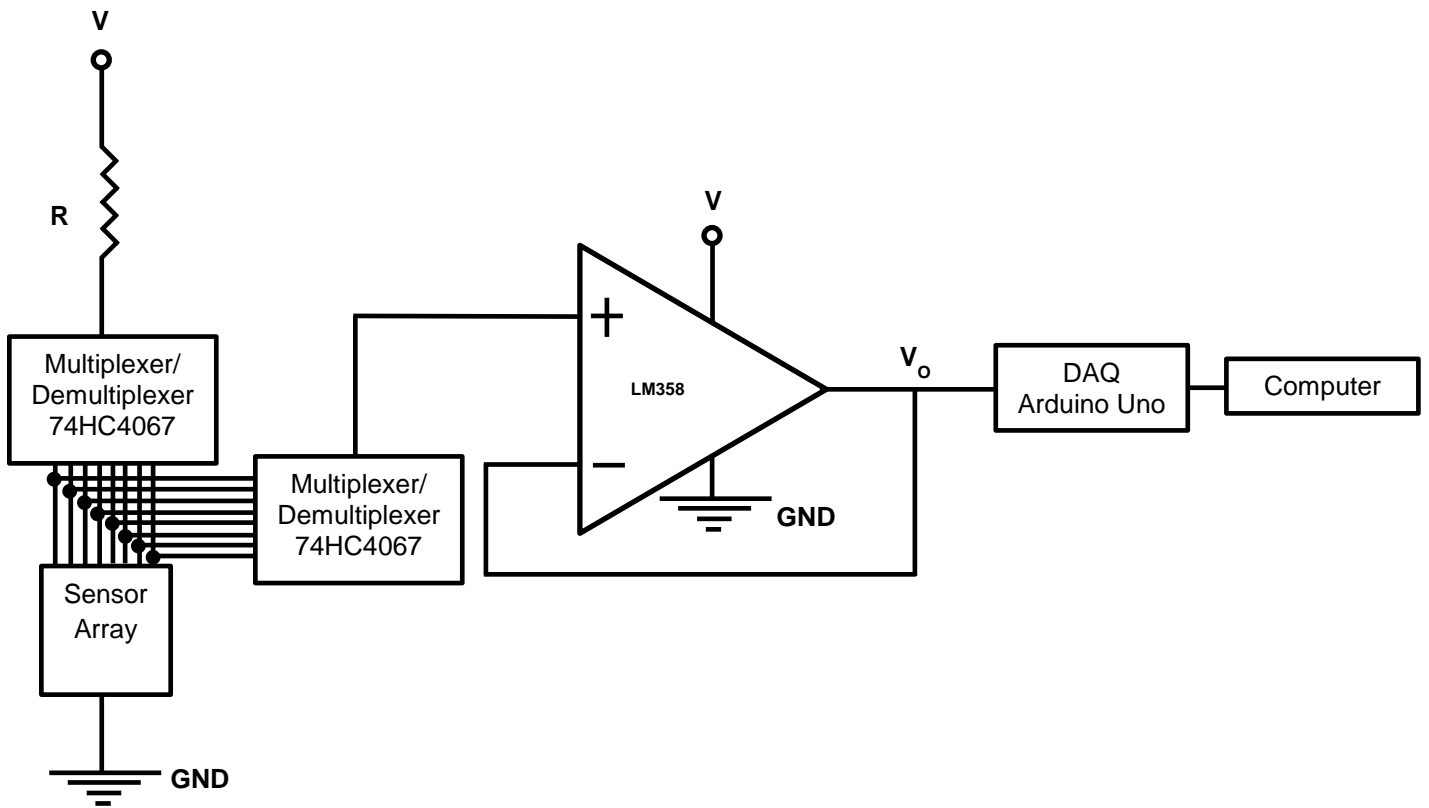
Hardik J. Pandya^{1,*}, Kihan Park¹, Wenjin Chen², Marina Chekmareva³, David Foran² and Jaydev P. Desai¹

* Correspondence to: hjpandya@umd.edu

Supplementary Methods

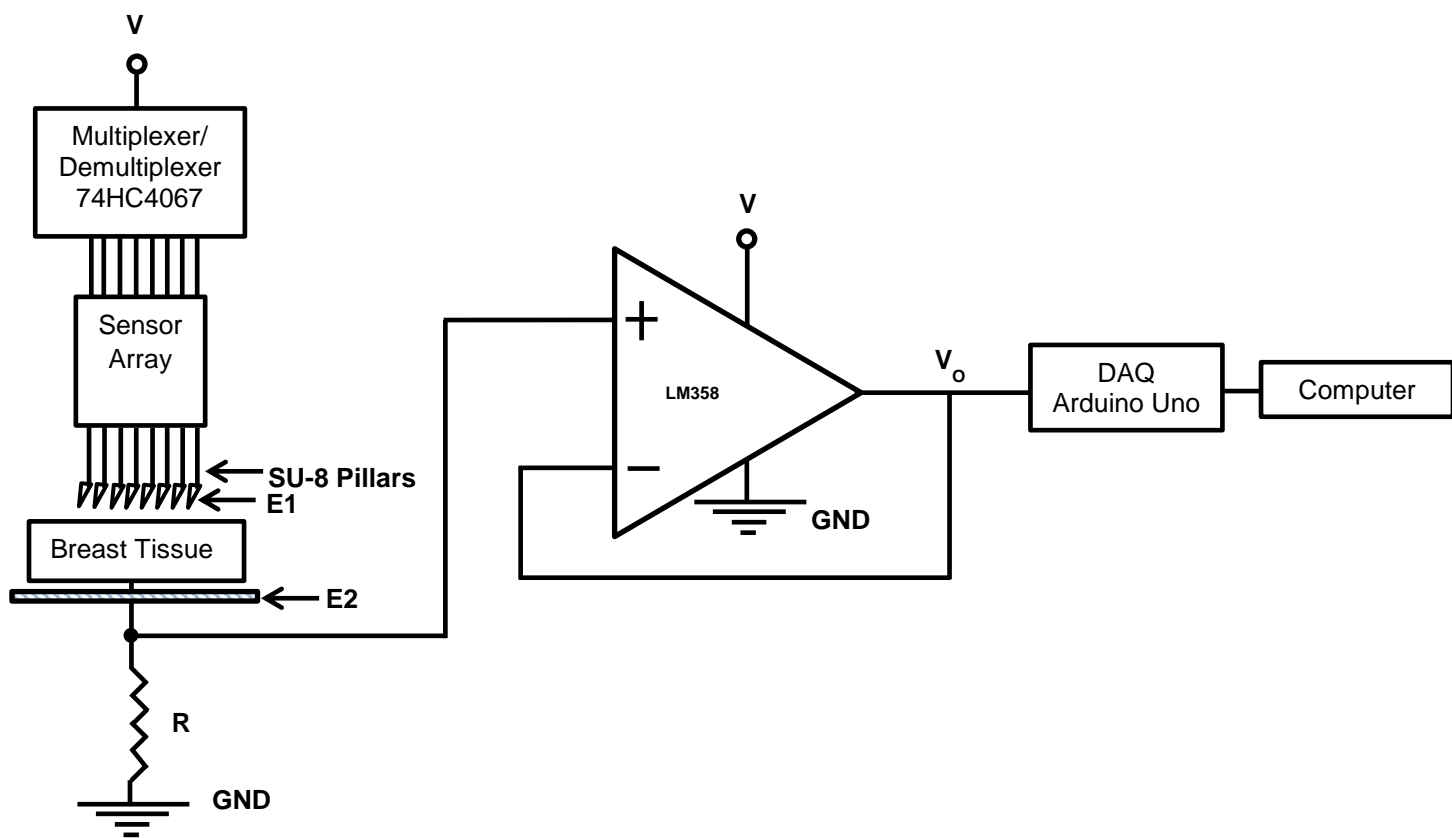


Supplementary Fig. S1. Tissue preparation: The H&E stained surface section of patient tissue block; 1 mm tissue core with specific histopathological feature was extracted. Consecutive sections of 10 μm and 4 μm thickness (as illustrated) were designated for subsequent steps in the experiment.



Supplementary Fig. S2. Electronic module. Displaying voltage as a function of the indentation of breast tissue.

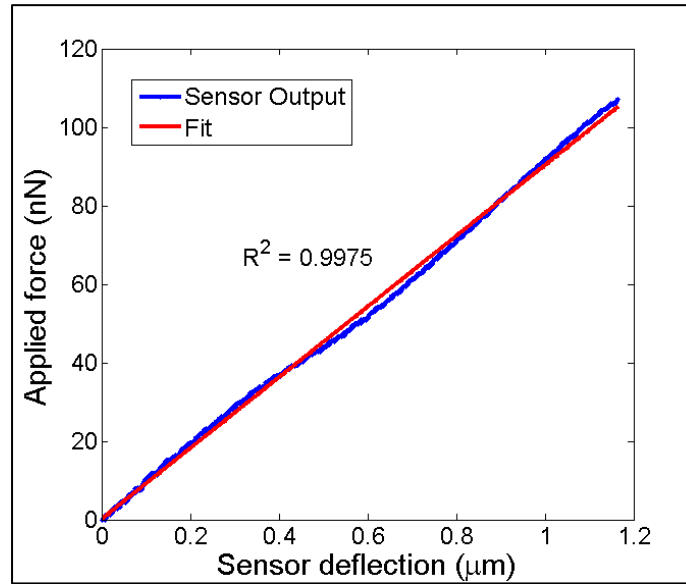
We have used a 10 bit analog-to-digital converter for the experiments. The resolution for the mechanical measurement is 4.15mV [defined as 5V (full scale range) divided by 1024 (2^{10})]. Though there are many ways to define the signal-to-noise ratio (SNR), an easier way to calculate SNR is to use the mean value and standard deviation (SD) of the measured voltage data, such that $SNR = MEAN/SD$. SNR is calculated as 45.24 ± 1.15 from the data of eight sensors at a stationary configuration without any contact with the tissue sample during 10 seconds with 100 Hz sampling rate.



Supplementary Fig. S3. Electronic module. Measuring electrical resistance of the breast tissue.

Sensor Calibration and Linear Regression Model

The fabricated sensors are calibrated in two stages before using it as a force sensing device to measure the mechanical properties of the breast tissue. In the first stage, the spring constant of each pillar in sensor array is determined using reference cantilever method^{1,2} and the relation between the sensor deflection and sensor output is determined. The AFM system (MFP-3D-BIOTM, Asylum Research, Inc.) is used for measuring spring constant. Figure S4 represents the force versus deflection curve of a pillar on the sensor array. The amount of sensor deflection is calculated as the difference between Z-direction movement and deflection of AFM tip. The mean value and standard deviation of spring constant for eight pillars is measured as 90.74 ± 3.90 nN/ μm , while the average R-square value is found to be 0.9975 ± 0.0021 .

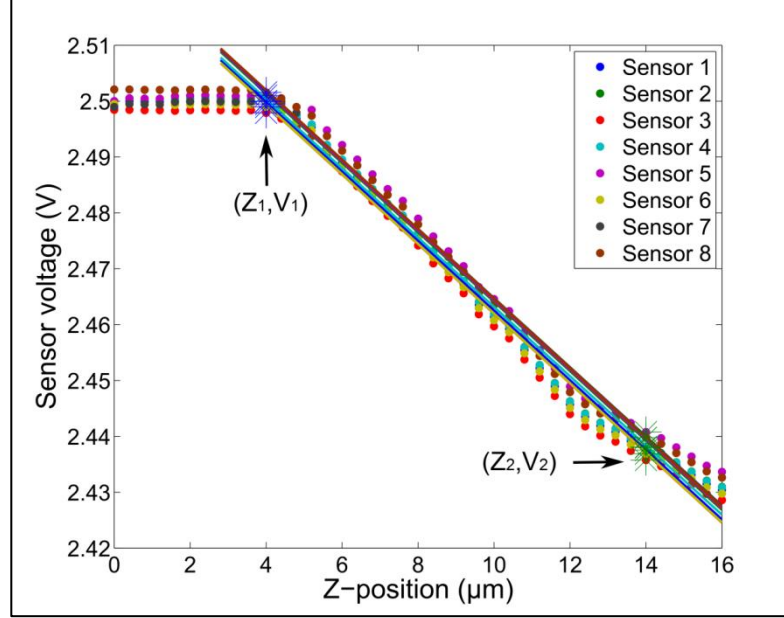


Supplementary Fig. S4. Spring constant measurement. The average value of spring constant for the sensor array was measured to be 90.74 ± 3.90 nN/ μm using reference cantilever method. The average R-square value was found to be 0.9975 ± 0.0021 which shows that the sensor array has a linear response.

The second stage of the sensor calibration is to measure the sensitivity of the sensor. The sensor is pressed on the glass and the corresponding change in sensor resistance is measured. This change in sensor resistance is due to the deformation in strain gauges. The sensor resistance is converted to voltage using a potential divider circuit. Thus, establishing a relation between piezoresistive sensor output voltage (V_{out}), change of sensor resistance (ΔR), and strain (ϵ) of the pillar that has linear relation with sensor deflection (δs), (i.e. $V_{\text{out}} \propto \Delta R \propto \epsilon \propto \delta s$). Therefore, the sensor output voltage can be mapped linearly with sensor deflection as given in equation (1).

$$V_{\text{out}} = \begin{cases} C_{11}(\delta_s) + C_{12}, & \text{Non - contact region} \\ C_{21}(\delta_s) + C_{22}, & \text{Contact region} \end{cases} \quad (1)$$

where, C_{11} , C_{12} , C_{21} , and C_{22} are coefficients from linear regression and δ_s is the sensor deflection. Figure S5 shows the change in sensor voltage with respect to sensor indentation on glass.



Supplementary Fig. S5. Sensitivity measurement of the fabricated sensor array. Measuring change in sensor voltage (V_{out}) as a function of the vertical distance (Z) by indenting the sensor on glass substrate.

To find the correlation between the change in sensor array to the sensor displacement, a linear regression model is used. The average goodness of fit (R^2 -value) for the sensor array is found to be 0.9890 ± 0.0014 . The sensitivity of the sensor is given by:

$$S = \frac{(V_2 - V_1)}{(Z_2 - Z_1)} \quad (2)$$

where, $V_2 = 2.4383$ V, $V_1 = 2.4999$ V, $Z_2 = 14$ μm , $Z_1 = 4$ μm .

The Z_1 , Z_2 , V_1 , and V_2 are the average values obtained from eight sensors. The sensitivity of sensor is measured to be 6.1532 ± 0.0991 mV/ μm .

Once the instantaneous sensor deflection is determined from the linear regression model at a certain point, the contact force between the sensor and the tissue is calculated as a product of spring constant obtained from the first calibration stage and the deflection of the sensor. The tissue deformation is measured using:

$$\delta_t = \Delta Z - \delta_s \quad (3)$$

where, δ_t is estimated tissue deformation, δ_s is the sensor deflection, and ΔZ is the difference between the initial z-position (when sensor makes contact with the tissue) and the final z-position of the micro-manipulator ($\sim 6\mu\text{m}$ in the present case).

The tissue elasticity is estimated by using Zhang's contact model³ with a cylindrical tip given by:

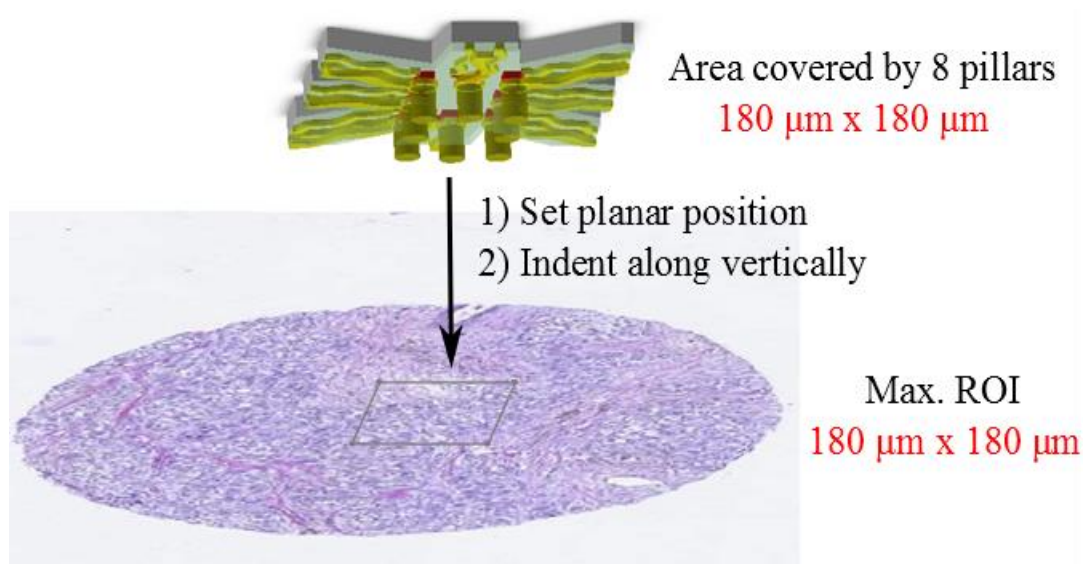
$$E = \frac{F(1-\nu^2)}{2r\kappa\delta_t} = \frac{k_s\delta_s(1-\nu^2)}{2r\kappa(\Delta Z - \delta_s)} \quad (4)$$

where, F is contact force, κ value is a function of Poisson's ratio (ν), ratio of indenter radius (r) to the thickness of tissue sample (h), and ratio of indentation depth to thickness of tissue sample. By using the table of κ -values and assuming that the tissue is incompressible, elasticity of the tissue can be determined.³

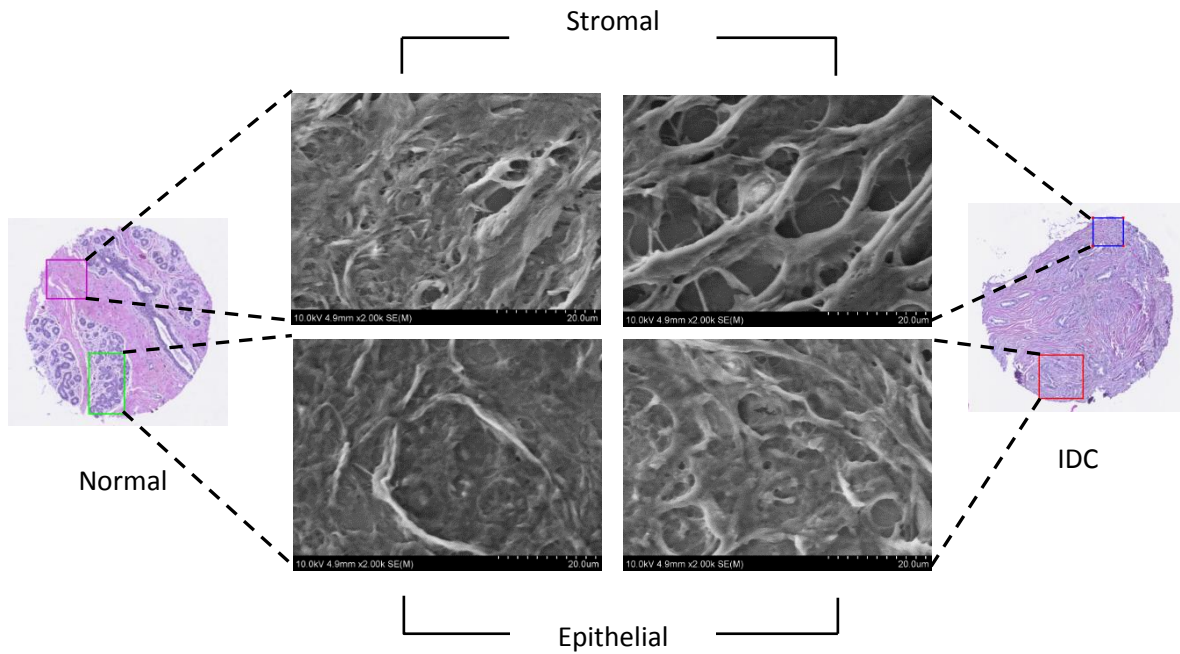
Electro-mechanical sensing methodology

The sensor is attached at the tip of micromanipulator with the configuration that the pillars are facing the tissue core on the bottom. By controlling micromanipulator, the sensor is moved in plane parallel with the sample tissue on to pre-defined ROI. Then, indentation along vertical direction is performed to make a right angle contact between the pillars and the tissue.

The location of the pillars on the sensor and the area covered by the pillars, matches with the pathological ROI ($180\mu\text{m} \times 180\mu\text{m}$). This design enables faster measurement by covering a larger ROI at once rather than a single probe used in an AFM. From a single measurement per tissue, we can obtain the data from 8 different regions within an ROI, which maps to eight points.



Supplementary Fig. S6. Electro-mechanical sensing methodology.

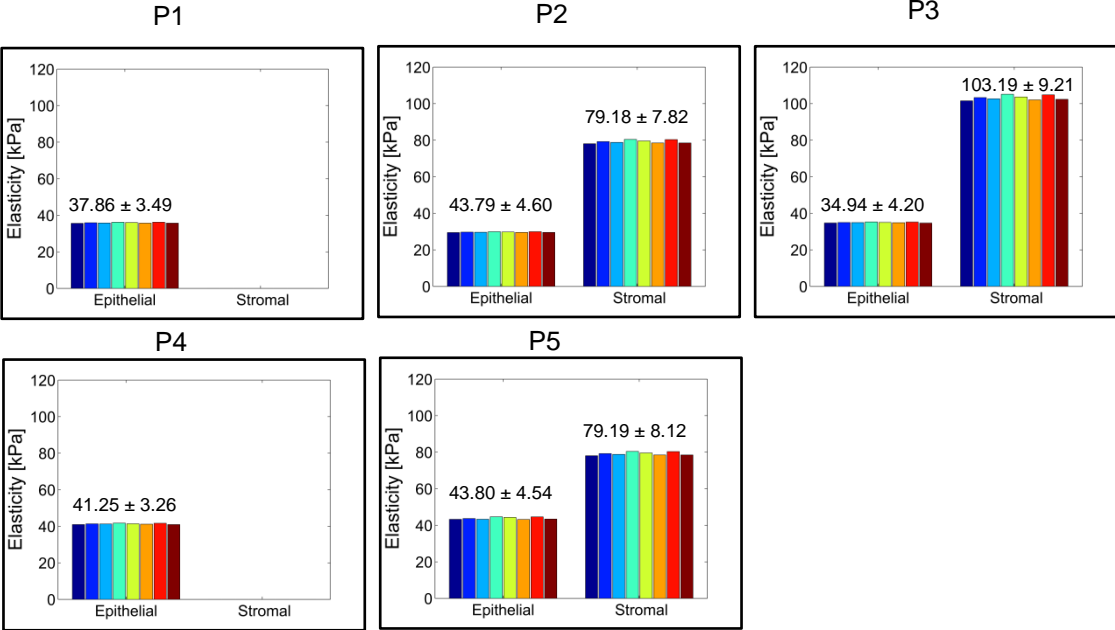


Supplementary Fig. S7. Field-emission scanning electron microscopy revealing microstructure of breast tissue cores.

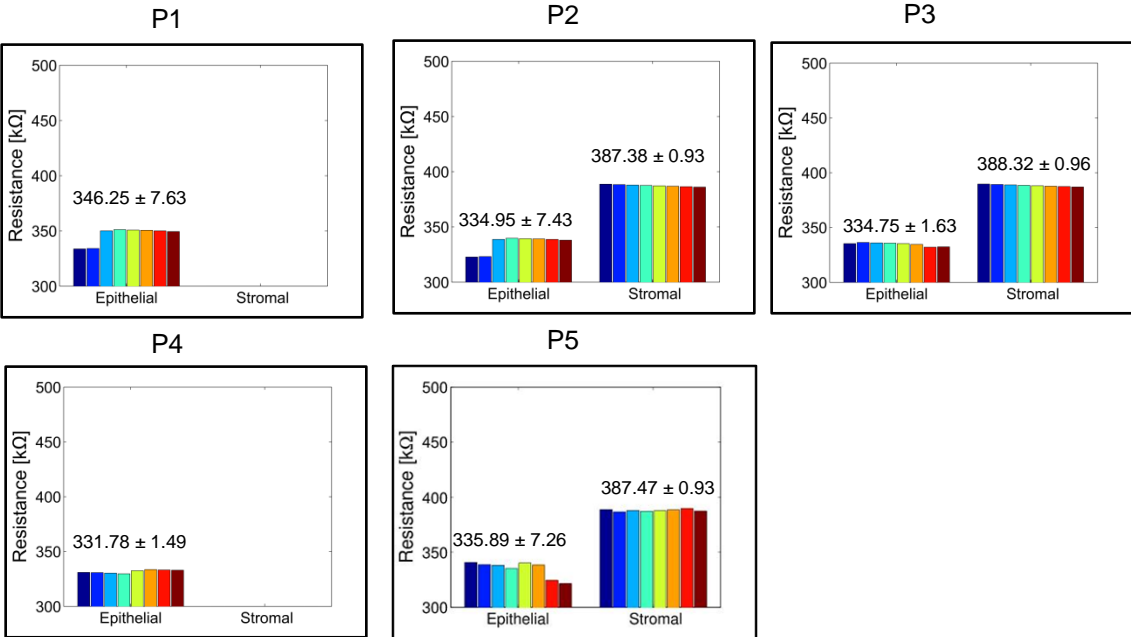
The FE-SEM image confirms the architectural changes in the breast tissue. The normal epithelial region shows an organized glandular structure with intact base membrane, while a delicate network of fibers can be seen in stromal region. In case of cancer, the stromal region was composed thick fiber bundles with increased fenestration and epithelial region shows a ruptured layer compared to normal epithelial region.

Normal Cases:

Mechanical Signatures:



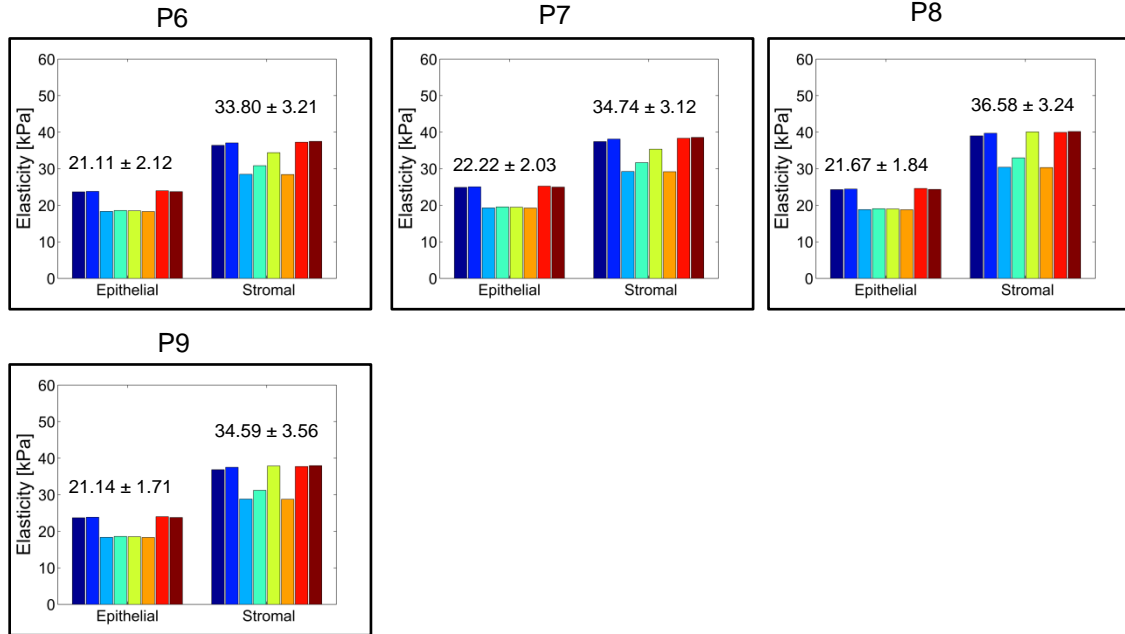
Electrical Signatures:



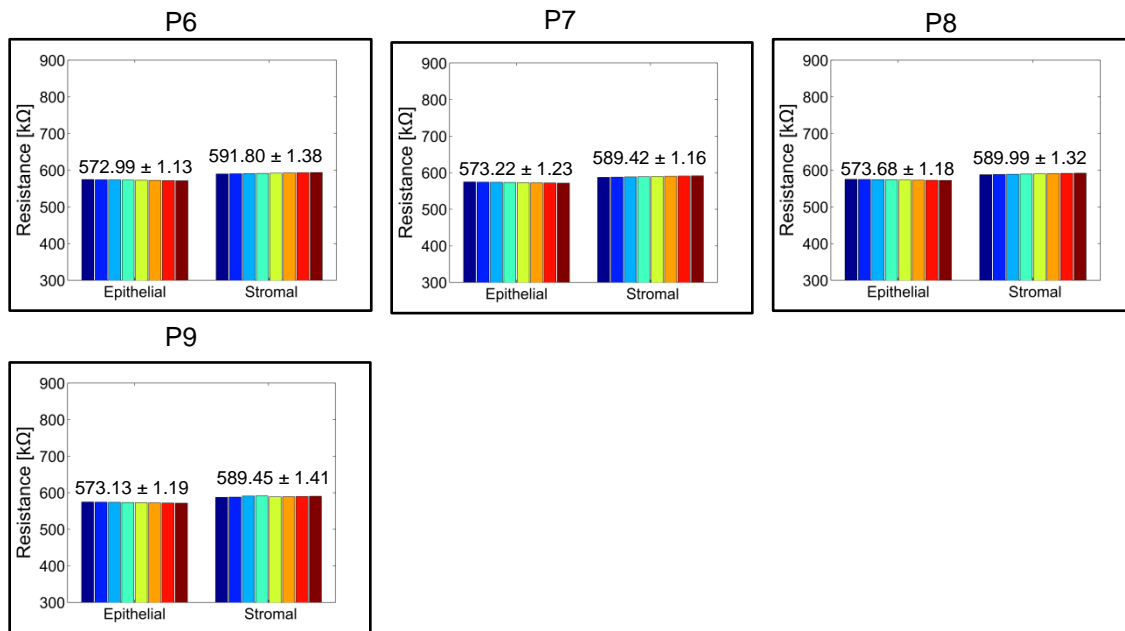
Cancer Cases:

Ductal Carcinoma in-Situ:

Mechanical Signatures:

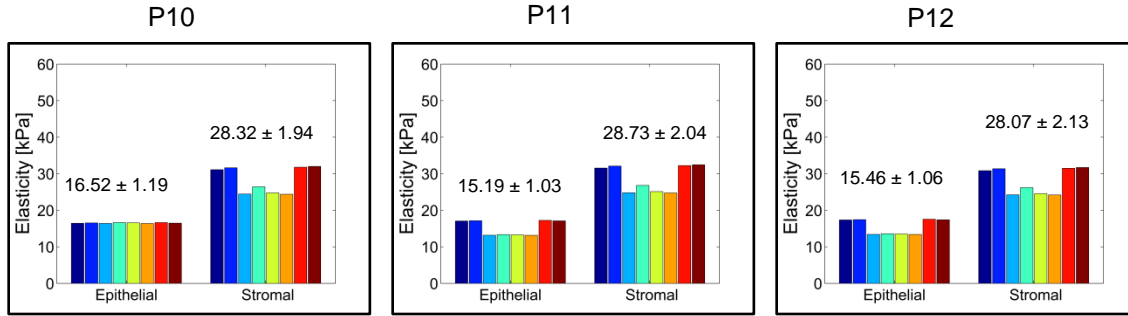


Electrical Signatures:

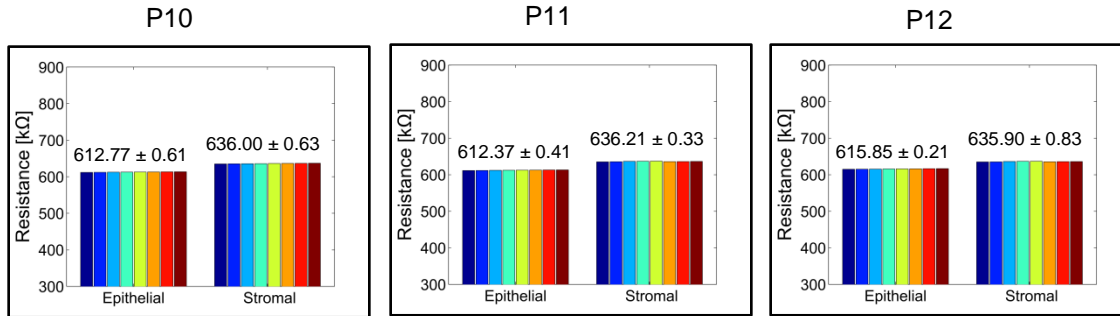


Lobular Carcinoma in-Situ:

Mechanical Signatures:

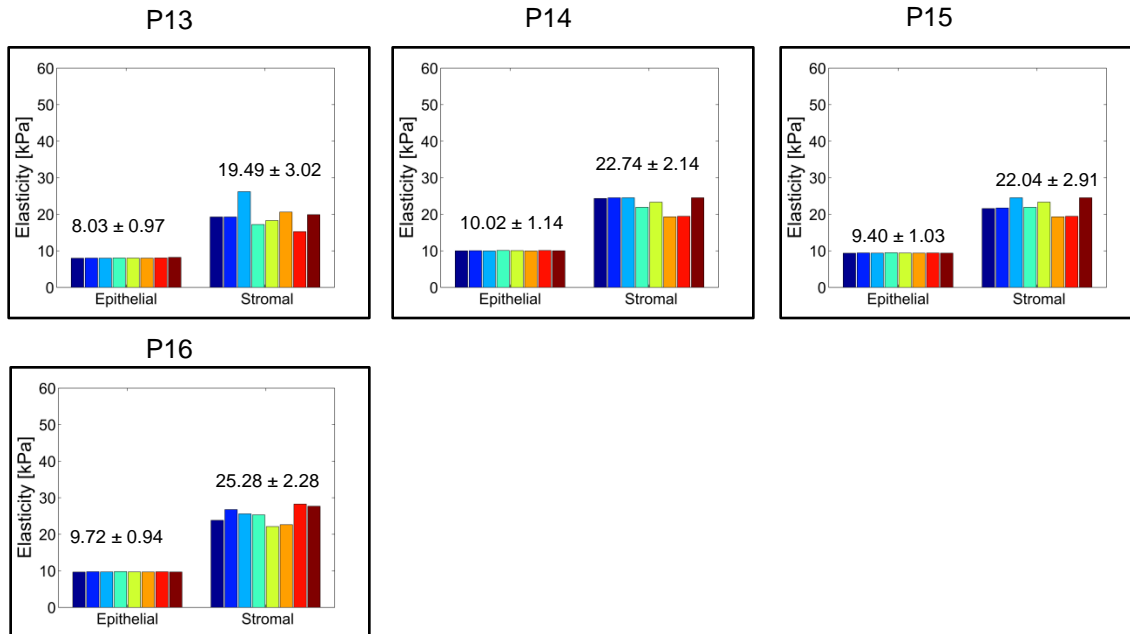


Electrical Signatures:

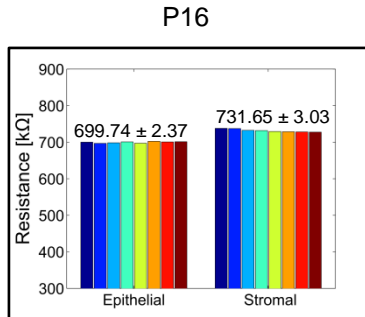
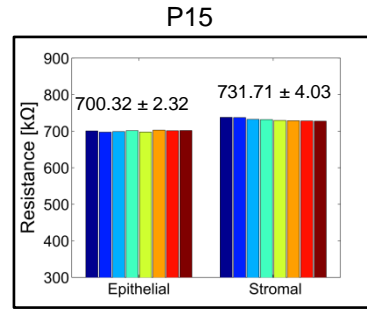
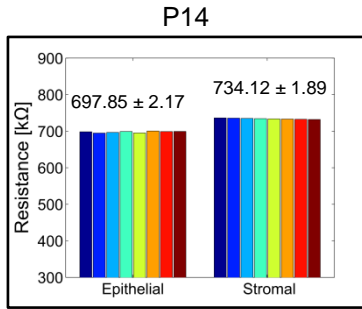
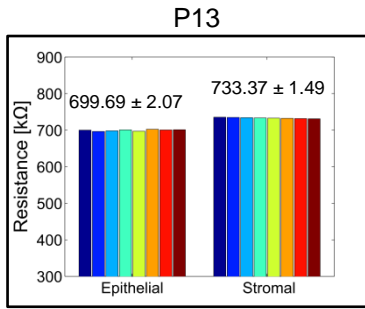


Invasive Ductal Carcinoma:

Mechanical Signatures:

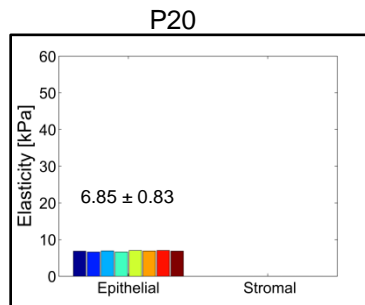
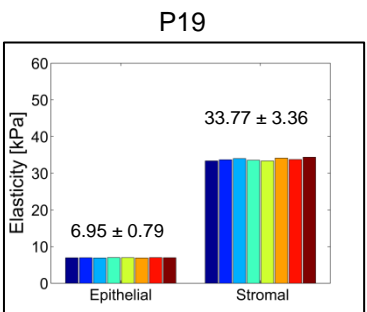
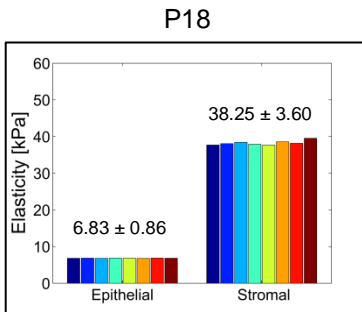
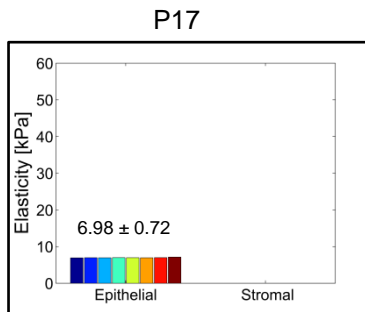


Electrical Signatures:

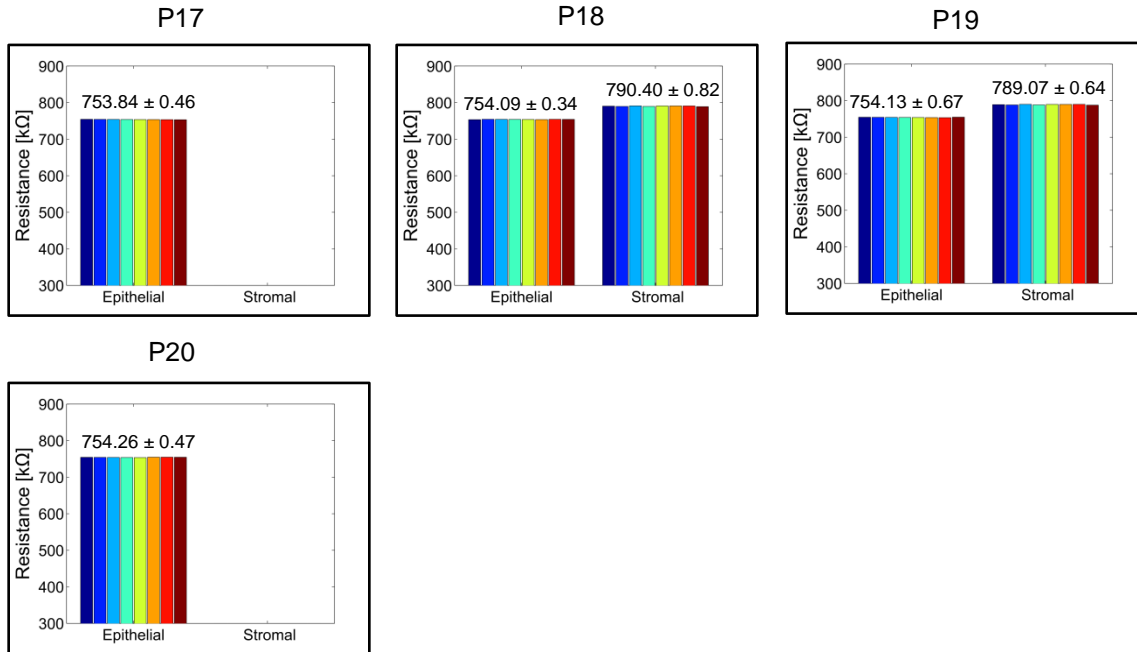


Invasive Lobular Carcinoma:

Mechanical Signatures:



Electrical Signatures:



Supplementary Fig. S8. Electro-mechanical properties of the breast tissue. The average value of the elasticity and electrical resistance measured by the sensor array for breast tissue core from each patient is listed in Supplementary Table S1. The elasticity and electrical resistance range (epithelial and stromal) of normal breast tissue cores (Patient 1 to Patient 5), ductal carcinoma in-situ (Patient 6 to Patient 9), lobular carcinoma in-situ (Patient 10 to Patient 12), invasive ductal carcinoma (Patient 13 to Patient 16) and invasive lobular carcinoma (Patient 17 to Patient 20) is listed in Table S2. The elasticity decreases and resistance of the breast tissue cores increases with progression of cancer. The stage of the cancer can be determined from the elasticity and measured electrical resistance of breast tissue cores in epithelial and stromal regions respectively. The values in each plot shows mean \pm standard deviation.

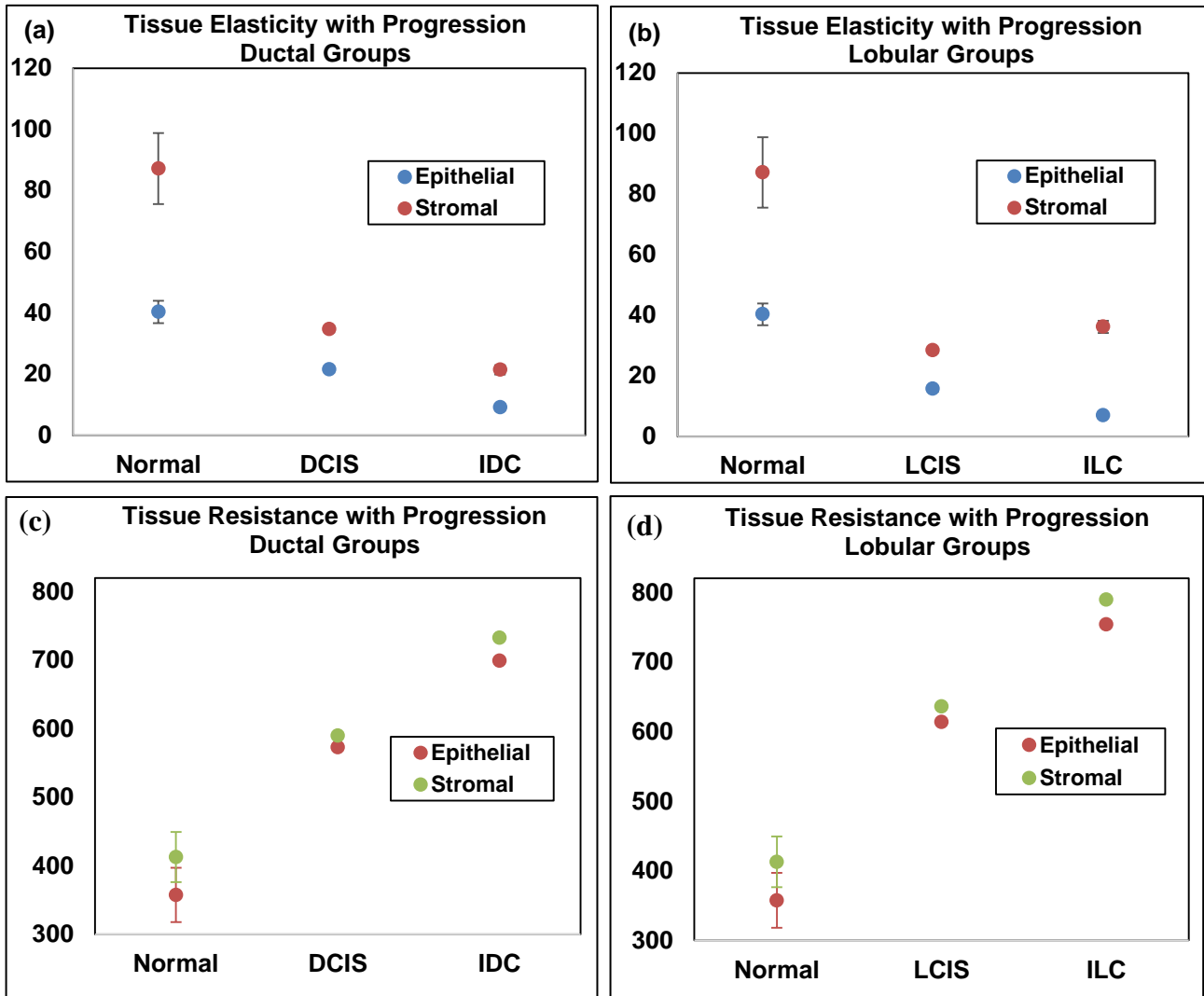
Table S1. Individual electrical (change in tissue resistance, mean \pm SD) and mechanical (elasticity E, mean \pm SD) analysis of breast tissue samples.

Patient no.	Block letter	BRS number	Age/Sex	Year of Tissue Collection	Mechanical Signature Mean value of elasticity (kPa) with standard deviation	Electrical Signature (Indentation 4 μm) Mean value of resistance (kΩ) with standard deviation	Region of Interest (ROI) (200x200 μm)	Pathological Status
P1	A	30365	39/female	2014	37.86 \pm 3.49	346.25 \pm 7.63	Epithelial	Normal
P2	B	28363	/female	2013	43.79 \pm 4.60	334.95 \pm 7.43	Epithelial	Normal
	B	28363	/female	2013	79.18 \pm 7.82	387.38 \pm 0.93	Stromal	Normal
P3	A	28480	31/female	2013	34.94 \pm 4.20	334.75 \pm 1.63	Epithelial	Normal
	A	28480	31/female	2013	103.19 \pm 9.21	388.32 \pm 0.96	Stromal	Normal
P4	A	28152	/female	2013	41.25 \pm 3.26	331.78 \pm 1.49	Epithelial	Normal
P5	A	31872	26/female	2014	43.80 \pm 4.54	335.89 \pm 7.26	Epithelial	Normal
	A	31872	26/female	2014	79.19 \pm 8.12	387.47 \pm 0.93	Stromal	Normal
P6	A	11809	78/female	2008	21.11 \pm 2.12	572.99 \pm 1.13	Epithelial	Ductal carcinoma In Situ (DCIS)
	A	11809	78/female	2008	33.80 \pm 3.21	591.80 \pm 1.38	Stromal	Ductal carcinoma In Situ (DCIS)
P7	A	29688	52/female	2013	22.22 \pm 2.03	573.22 \pm 1.23	Epithelial	Ductal carcinoma In Situ (DCIS)
	A	29688	52/female	2013	34.74 \pm 3.12	589.42 \pm 1.16	Stromal	Ductal carcinoma In Situ (DCIS)
P8	A	28453	47/female	2013	21.67 \pm 1.84	573.68 \pm 1.18	Epithelial	Ductal carcinoma In Situ (DCIS)
	A	28453	47/female	2013	36.58 \pm 3.24	589.99 \pm 1.32	Stromal	Ductal carcinoma In Situ (DCIS)
P9	A	25043	89/female	2012	21.14 \pm 1.71	573.13 \pm 1.19	Epithelial	Ductal carcinoma In Situ (DCIS)
	A	25043	89/female	2012	34.59 \pm 3.56	589.45 \pm 1.41	Stromal	Ductal carcinoma In Situ (DCIS)
P10	A	27928	46/female	2013	16.52 \pm 1.19	612.77 \pm 0.61	Epithelial	Lobular carcinoma In Situ (LCIS)
	A	27928	46/female	2013	28.32 \pm 1.94	636.00 \pm 0.63	Stromal	Lobular carcinoma In Situ (LCIS)
P11	A	11223	65/female	2007	15.19 \pm 1.03	612.37 \pm 0.41	Epithelial	Lobular carcinoma In Situ (LCIS)
	A	11223	65/female	2007	28.73 \pm 2.04	636.21 \pm 0.33	Stromal	Lobular carcinoma In Situ (LCIS)
P12	A	25350	70/female	2012	15.46 \pm 1.06	615.85 \pm 0.21	Epithelial	Lobular carcinoma In Situ (LCIS)
	A	25350	70/female	2012	28.07 \pm 2.13	635.90 \pm 0.83	Stromal	Lobular carcinoma In Situ (LCIS)
P13	A	29689	52/female	2013	8.03 \pm 0.97	699.69 \pm 2.07	Epithelial	Invasive ductal carcinoma (IDC)
	A	29689	52/female	2013	19.49 \pm 3.02	733.37 \pm 1.49	Stromal	Invasive ductal carcinoma (IDC)
P14	A	26249	67/female	2012	10.02 \pm 1.14	697.85 \pm 2.17	Epithelial	Invasive ductal carcinoma (IDC)
	A	26249	67/female	2012	22.74 \pm 2.14	734.12 \pm 1.89	Stromal	Invasive ductal carcinoma (IDC)

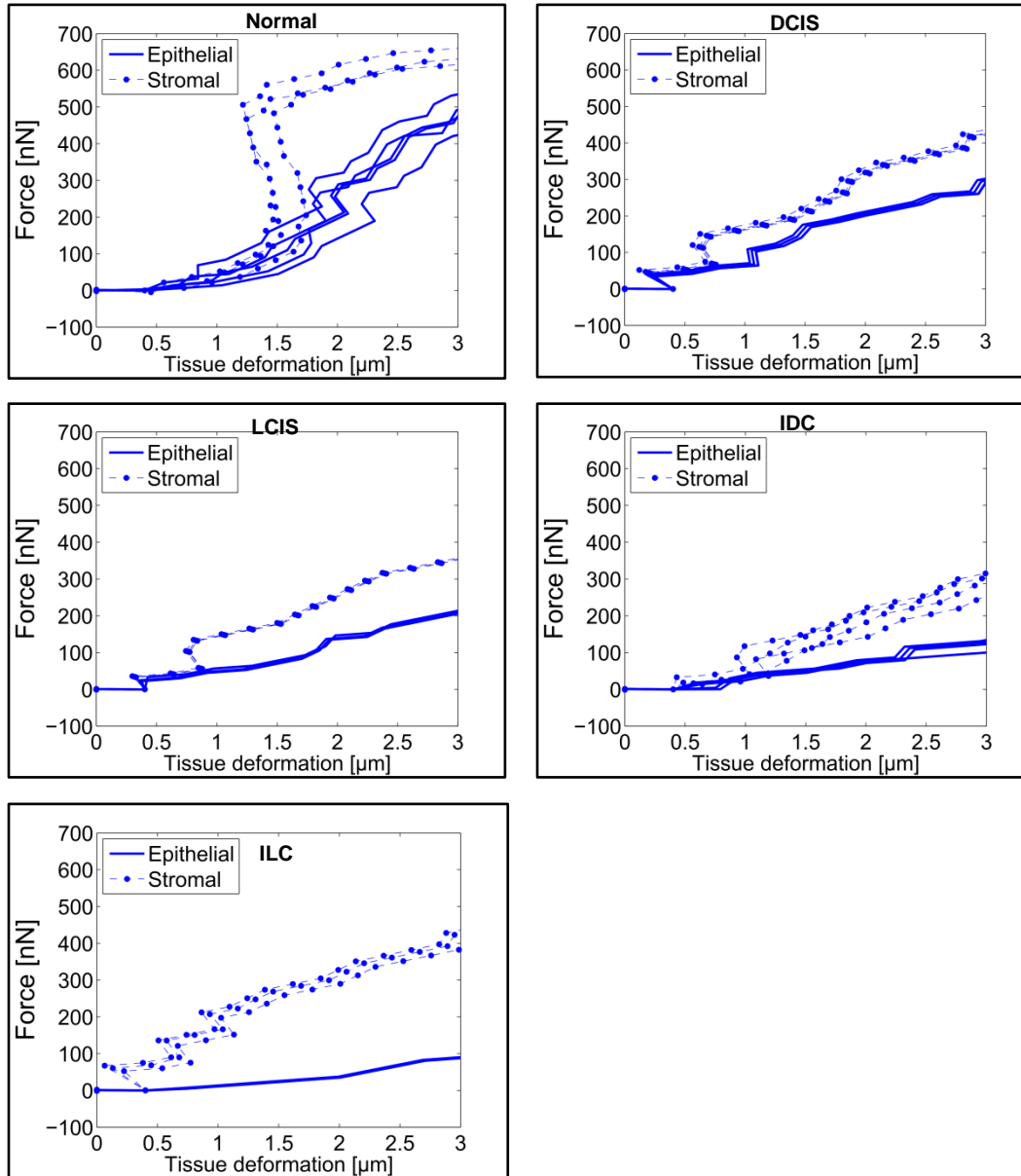
Patient no.	Block letter	BRS number	Age/Sex	Year of Tissue Collection	Mechanical Signature Mean value of elasticity (kPa) with standard deviation	Electrical Signature (Indentation 4 μm) Mean value of resistance (kΩ) with standard deviation	Region of Interest (ROI) (200x200 μm)	Pathological Status
P15	C	17316	51/female	2010	9.40 \pm 1.03	700.32 \pm 2.32	Epithelial	Invasive ductal carcinoma (IDC)
	C	17316	51/female	2010	22.04 \pm 2.91	731.71 \pm 4.03	Stromal	Invasive ductal carcinoma (IDC)
P16	B	27952	31/female		9.72 \pm 0.94	699.74 \pm 2.37	Epithelial	Invasive ductal carcinoma (IDC)
	B	27952	31/female		25.28 \pm 2.28	731.65 \pm 3.03	Stromal	Invasive ductal carcinoma (IDC)
P17	A	19306	78/female	2010	6.98 \pm 0.72	753.84 \pm 0.46	Epithelial	Invasive Lobular carcinoma (ILC)
P18	B	11223	65/female	2007	6.83 \pm 0.86	754.09 \pm 0.34	Epithelial	Invasive Lobular carcinoma (ILC)
	A	11223	65/female	2007	38.25 \pm 3.60	790.40 \pm 0.82	Stromal	Invasive Lobular carcinoma (ILC)
P19	A	26763	/female	2012	6.95 \pm 0.79	754.13 \pm 0.67	Epithelial	Invasive Lobular carcinoma (ILC)
	A	26763	/female	2012	33.77 \pm 3.36	789.07 \pm 0.64	Stromal	Invasive Lobular carcinoma (ILC)
P20	A	25350	70/female	2012	6.85 \pm 0.83	754.26 \pm 0.47	Epithelial	Invasive Lobular carcinoma (ILC)

Table S2. Group-wise distribution of the elasticity and tissue resistance range for normal and cancerous breast tissue samples.

Type of Breast Tissue	Region	Elasticity (kPa)	Resistance (kΩ)
Normal	Epithelial	34.94 ± 4.20 to 43.80 ± 4.54	331.78 ± 1.49 to 346.25 ± 7.63
	Stromal	79.18 ± 7.82 to 103.19 ± 9.21	387.38 ± 0.93 to 388.32 ± 0.96
Ductal carcinoma In Situ (DCIS)	Epithelial	21.11 ± 2.12 to 22.22 ± 2.03	572.99 ± 1.13 to 573.68 ± 1.18
	Stromal	33.80 ± 3.21 to 36.58 ± 3.24	589.42 ± 1.16 to 591.80 ± 1.38
Lobular carcinoma In Situ (LCIS)	Epithelial	15.19 ± 1.03 to 16.52 ± 1.19	612.77 ± 0.61 to 615.85 ± 0.21
	Stromal	28.07 ± 2.13 to 28.73 ± 2.04	635.90 ± 0.83 to 636.21 ± 0.33
Invasive ductal carcinoma (IDC)	Epithelial	8.03 ± 0.97 to 10.02 ± 1.14	697.85 ± 2.17 to 700.32 ± 2.32
	Stromal	19.49 ± 3.02 to 25.28 ± 2.28	731.71 ± 4.03 to 734.12 ± 1.89
Invasive Lobular carcinoma (ILC)	Epithelial	6.83 ± 0.86 to 6.98 ± 0.72	753.84 ± 0.46 to 754.26 ± 0.47
	Stromal	33.77 ± 3.36 to 38.25 ± 3.60	788.41 ± 0.92 to 790.40 ± 0.82



Supplementary Fig. S9. Statistical Analysis. Elastic Modulus and electrical resistance of tumors from ductal and lobular groups relative to normal breast tissue.



Supplementary Fig. S10. Force curves from breast tissue cores. Force curves obtained from epithelial and stromal region of **a**, normal, **b**, ductal carcinoma in-situ, **c**, lobular carcinoma in-situ, **d**, invasive ductal carcinoma and **e**, lobular invasive carcinoma breast tissues. Distinct force profiles are obtained from each core.

References

1. Cumpson, P.J., Clifford, C.A., Hedley, J. Quantitative analytical atomic force microscopy: a cantilever reference device for easy and accurate AFM spring-constant calibration. *Meas. Sci. Technol.* 2004, **15**, 1337-1346.
2. Hutter, J., Bechhoeffer, J. Calibration of atomic-force microscope tips. *Rev. Sci. Instrum.* 1993, **64(7)**, 1868-1873.
3. Zhang M., Zheng, Y. P., Mak, A.F.T. Estimating the Effective Young's Modulus of Soft Tissues from Indentation Tests—Nonlinear Finite Element Analysis of Effects of Friction and Large Deformation. *Med. Eng. Phys.* 1997, **19**, 512-517.